Exp Brain Res (2004) 157: 507–517
DOI 10.1007/s00221-004-1864-7

RESEARCH ARTICLES

Eric J. Perreault · Robert F. Kirsch · Patrick E. Crago

Multijoint dynamics and postural stability of the human arm

Received: 6 October 2003 / Accepted: 7 January 2004 / Published online: 27 April 2004

Abstract The goal of this study was to examine how the mechanical properties of the human arm are modulated during isometric force regulation tasks. Specifically, we examined whether the dynamic stability of the limb remained nearly invariant across a range of voluntarily generated endpoint forces and limb postures. Previous single joint studies have demonstrated that dynamic joint stability, as quantified via estimates of the joint damping ratio, is nearly invariant during isometric torque regulation tasks. However, the relevance of these findings to the control of multijoint posture has not been investigated previously. A similar degree of invariance at the multijoint level could suggest a fundamental property of the motor system that could be incorporated into the planning and execution of multijoint tasks. In this work, limb mechanics were quantified using estimates of dynamic endpoint stiffness, which characterizes the relationship between imposed displacements of limb posture and the forces opposing those displacements. Endpoint stiffness was estimated using a two-link robot operating in the horizontal plane at the height of each subject's glenohumeral joint. The robot was used to apply stochastic position perturbations to the arm and to measure the resulting forces. Endpoint stiffness dynamics were estimated nonparametrically and subsequently summarized using inertial, viscous and elastic parameters. We found that in the tasks studied, there was a differential modulation of endpoint elasticity and endpoint viscosity. Elasticity increased nearly linearly with increases in voluntary force generation while viscosity increased nonlinearly. This differential regulation resulted in limb dynamics that had a remarkably consistent damping ratio across all subjects and all tested conditions. These results emphasize the importance of considering the full dynamic response of a limb when investigating multijoint stability, and suggest that a minimal degree of limb stability is maintained over a wide range of force regulation tasks.

Keywords Limb stiffness · Multijoint mechanics · Impedance · Postural stability · Biomechanics

This work was supported by the Department of Veteran Affairs Rehabilitation Research and Development Service, the National Institute of Health, and the Cleveland FES Institute

E. J. Perreault (✉)
Department of Biomedical Engineering and Department of Physical Medicine and Rehabilitation, Northwestern University,
345 E. Superior St., Room 1403,
Chicago, IL 60611, USA
e-mail: e-perreault@northwestern.edu
Fax: +1-312-2382208

R. F. Kirsch · P. E. Crago
Department of Biomedical Engineering, Case Western Reserve University,
Cleveland, OH, USA

R. F. Kirsch · P. E. Crago
Louis Stokes VA Medical Center,
Cleveland, OH, USA

Introduction

Maintaining stable arm postures during a task requires both the strength to complete the task and the stability to reject external disturbances that might be encountered during task completion. Strength and stability are regulated via changes in muscle activation. However, co-contraction of antagonistic muscles allows these factors to be modulated independently; increased co-contraction decreases the net strength or external forces generated by the arm while simultaneously increasing whole limb stability. The purpose of this study was to quantify how limb stability was regulated during isometric force regulation tasks. These tasks consist of exerting steady state forces against a rigid interface. Understanding how the central nervous system regulates strength and stability during such tasks may elucidate strategies used in the control of posture and provide a set of baseline data for investigating how these strategies change during more complex tasks such as movement or object manipulation.

Limb stability can be quantified using estimates of dynamic endpoint stiffness, which describes the relation-

ship between externally imposed displacements of the hand and the forces generated in response. As such, it represents a measure of the mechanical interface that the arm presents to its environment. For small perturbations about a given posture, dynamic stiffness can be approximated by the inertial, viscous and elastic properties of the arm (Dolan et al. 1993; Lacquaniti et al. 1993; Tsuji et al. 1995; Perreault et al. 1999; Stroeve 1999). The viscous and elastic components of limb stiffness can be modified by changes in muscle activation, providing a mechanism by which the central nervous system can regulate limb mechanics and stability. Hogan (1985) first proposed that the central nervous system could maintain arm stability via regulation of its endpoint stiffness properties. This has led to numerous investigations into the control of multijoint stiffness properties. However, most of these studies have focused on the elastic components of endpoint stiffness (Mussa-Ivaldi et al. 1985; McIntyre et al. 1996; Flash and Gurevich 1997; Perreault et al. 2001). While these components are essential for maintaining steady state stability, the inertial and viscous properties also contribute to the dynamic stability. A few studies have quantified the viscous and inertial properties of multijoint systems (Dolan et al. 1993; Lacquaniti et al. 1993; Tsuji et al. 1995; Gomi and Osu 1998), but none has examined the net influence of these properties on whole limb stability and the dynamic response to external perturbations of limb posture. In contrast, several studies have investigated the dynamic stability of single joint systems (Agarwal and Gottlieb 1977; Weiss et al. 1988; Sinkjaer and Hayashi 1989). This has been accomplished by computing the damping ratio of the joint. The damping ratio quantifies the degree to which a system will oscillate once perturbed. A remarkable consistency in the damping of individual joints has been reported during single joint torque regulation tasks, suggesting an invariant characteristic during the maintenance of posture.

The goal of this study was to examine how the limb inertia, viscosity and elasticity are modulated during isometric force regulation tasks and to quantify how these components contribute to the net stability of the limb. Based upon the results of single-joint studies, our hypothesis was that whole limb stability would remain nearly invariant over a wide range of arm postures and voluntarily generated forces. Results are discussed in the context of how multijoint stability may be regulated during the normal control of movement and posture.

Methods

Experimental

Apparatus

Endpoint stiffness was estimated using perturbations applied by a two-joint robotic manipulator described in detail previously (Acosta et al. 2000) and summarized briefly below. Figure 1 illustrates this device, which was configured as a position servo for these experiments. Subjects were strapped into a rigid chair with custom supports to constrain both lateral and anterior-posterior trunk movements. Each subject's arm was attached to the manipulator endpoint via a custom-fitted fiberglass cast that was free to pivot in the horizontal plane about the attachment point. Each subject's cast rigidly fixed the wrist joint and covered approximately three-quarters of the forearm. The manipulator was instrumented to measure the displacements of the subject's hand and the forces applied between the subject and the manipulator.

Subjects and protocol

Five healthy subjects ranging from 22 to 40 years old and with no history of neurological impairments were used in this study. Subjects gave informed consent to all procedures and were free to withdraw from the study at any time. The subject protocols were approved by the MetroHealth Medical Center Institutional Review Board (protocol number: 09423-ORTH-94).

To observe how endpoint stiffness varied as a function of endpoint location, measurements were made at three locations in a horizontal workspace at the vertical level of the glenohumeral joint. All positions were approximately 0.3 m anterior to the acromion. The medial position (M) was in front of the sternum, the central position (C) in front of the acromion, and the lateral position (L) approximately 0.2 m to the right of the acromion. Subjects were secured in the experimental apparatus at the approximate locations described above; the resulting joint angles and endpoint locations were then digitized using an Optotrak system [Northern Digital, Waterloo, Ontario]. Table 1 gives the measured joint angles and endpoint locations for each subject. All measurements were made on the right arm, which happened to be the dominant arm of each subject.

Prior to each experiment, twelve maximum voluntary contractions (MVCs) were measured for each subject. These corresponded to the maximum endpoint force generated in four directions (parallel to the $\pm X$- and $\pm Y$-axes shown in Fig. 1) at each of the three endpoint locations. The minimum of these 12 MVCs was used to scale the subjects' voluntary effort in all remaining trials. Table 1 provides the

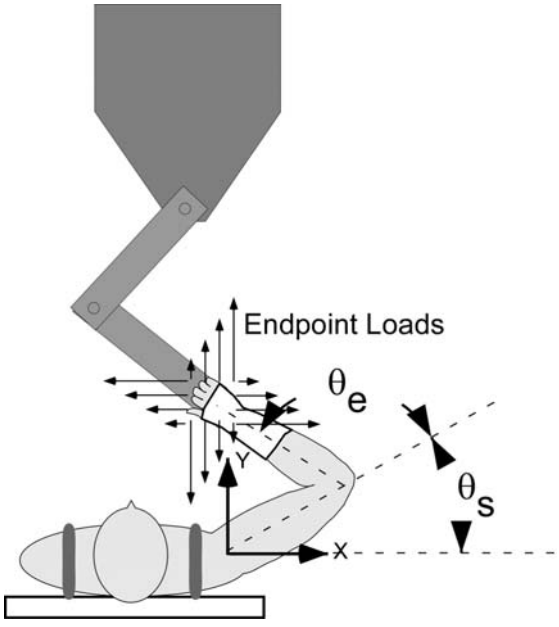

Fig. 1 A two-joint robotic manipulator was used to apply endpoint perturbations in these experiments. The manipulator was mounted on an adjustable structure, allowing its height to be customized for each subject. During each trial, subjects exerted a constant force on the manipulator in one of the four directions shown. Force magnitudes ranged from 0% to 30% MVC

Table 1 Subject-dependent experimental parameters, showing the humeral length (L_h) and forearm length (L_f) for each subject, as well as the joint angles and corresponding endpoint locations for each tested arm posture. *Rightmost column* provides the maximum endpoint force tested for each subject. This was 30% of each subject's MVC, as described in the text

Subject	Link lengths (m)		Arm orientation (deg, m)												Maximum tested load (N)
			Medial				Central				Lateral				
	L_h	L_f	θ_s	θ_e	x	y	θ_s	θ_e	x	y	θ_s	θ_e	x	y	
1	0.33	0.32	62.8	102.4	−0.16	0.37	41.7	103.3	−0.02	0.40	14.1	103.8	0.17	0.36	60
2	0.27	0.30	46.8	115.5	−0.10	0.29	21.4	120.6	0.01	0.28	−2.5	102.5	0.21	0.29	24
3	0.29	0.33	48.0	112.8	−0.12	0.33	19.5	117.9	0.03	0.32	3.5	99.2	0.22	0.34	54
4	0.30	0.32	47.1	121.9	−0.11	0.28	23.3	124.6	0.01	0.29	−3.5	111.0	0.20	0.29	45
5	0.34	0.33	57.7	119.8	−0.15	0.30	27.2	120.5	0.02	0.33	−1.6	111.3	0.23	0.30	72

maximum force (30% MVC in the weakest direction) used for each subject.

During each trial, subjects were instructed to exert a constant force against the manipulator in one of the four directions shown in Fig. 1 (±*X* and ±*Y*). For each direction, the same four force magnitudes were tested: 7.5, 15, 22.5, and 30% MVC (of the weakest direction). In addition, one trial was performed while the subject was at rest, exerting no voluntary endpoint force on the manipulator. Subjects were assisted in this task by a visual display of the endpoint force and the force target.

Figure 2A shows typical endpoint displacements and forces recorded for a single trial during which the subject exerted a constant voluntary force in the –*Y* direction. Each trial lasted for 41 s. Data from the first 2 s (*a*) were used to record baseline values. At 2 s, an auditory cue instructed the subject to generate a predetermined endpoint force. The subject was given 4 s (*b*) to reach this specified target, after which the manipulator applied a stochastic position perturbation to the subject's hand. The final 30 s of data (*c*) was used for dynamic stiffness estimation. The applied displacement perturbations had peak-to-peak amplitudes of approximately 2 cm in each direction. The corresponding endpoint force amplitudes varied from trial to trial depending upon arm stiffness. The endpoint displacement frequency content was designed to be within the range of physiologically encountered perturbations (Mann et al. 1989) yet contain enough information for adequate identification of the endpoint dynamics. Figure 2B shows the spectra of the endpoint perturbations used in this study. These perturbations were flat to 3 Hz, above which they decayed at a rate of 40 dB/decade.

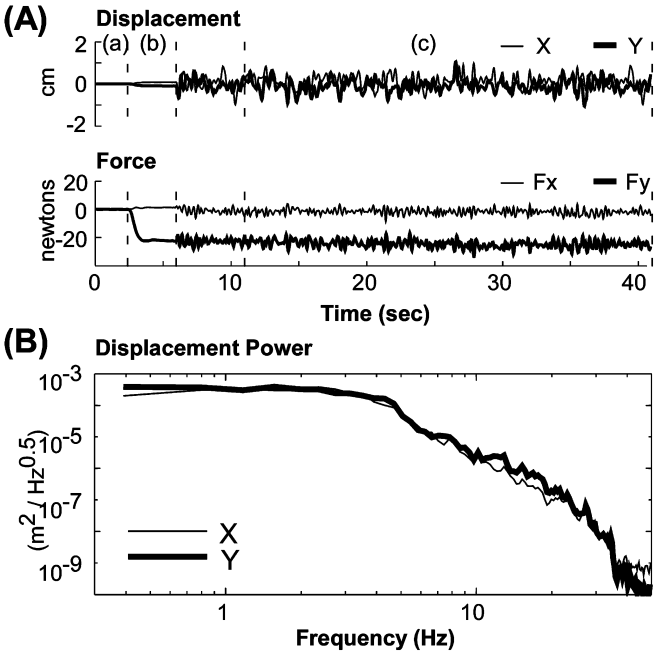

Fig. 2A, B Typical data from a single experimental trial. **A** shows typical endpoint displacements and forces. Data from the first 2 s *(a)* in each trial were used to record baseline values. After 2 s, an auditory cue instructed the subject to generate an endpoint force to match the target force. The subject was given 4 s *(b)* to reach the force target, after which the manipulator applied a stochastic position perturbation to the subject's hand. The final 30 s of data *(c)* were used for dynamic stiffness estimation. **B** shows the power spectrum of the applied position perturbations

Analytical

Nonparametric endpoint stiffness estimation

Endpoint stiffness describes the dynamic relationship between displacements imposed at the hand and the forces resisting those displacements. The measurements in these experiments were restricted to the horizontal plane, so the goal of the analysis procedures was to estimate the dynamic relationship between endpoint displacements and endpoint forces in the horizontal plane.

Stiffness dynamics were estimated using a robust and efficient nonparametric system identification algorithm described previously (Perreault et al. 1999). The primary assumption of this algorithm is that the endpoint stiffness dynamics can be approximated by a linear system for small perturbations of hand posture (Dolan et al. 1993; Tsuji et al. 1995; Stroeve 1999; Perreault et al. 2001). In general, any linear multiple-input, multiple-output (MIMO) system can be decomposed into the linear subsystems relating each input to each output. The dynamics equations describing the relationship between endpoint displacements and endpoint forces can be expressed succinctly in the frequency domain by Eq. 1, where f is frequency, $F_x(f)$ and $F_y(f)$ are the Fourier transforms of the endpoint forces, $X(f)$ and $Y(f)$ are the Fourier transforms of the endpoint displacements, and $H_{ij}(f)$ is the transfer function relating displacements in direction j to forces in direction i. The nonparametric algorithm estimates the optimal (least squares) linear model for each of these single-input, single-output (SISO) subsystems.

$$\begin{bmatrix} F_x(f) \\ F_y(f) \end{bmatrix} = \begin{bmatrix} H_{xx}(f) & H_{xy}(f) \\ H_{yx}(f) & H_{yy}(f) \end{bmatrix} \begin{bmatrix} X(f) \\ Y(f) \end{bmatrix} \quad (1)$$

The overall nonparametric fit for each data set was evaluated using the multiple correlation coefficient, R^2, defined in Eq. 2. $f_i(t)$ denotes the measured endpoint forces, $\hat{f}_i(t)$ denotes those predicted from the measured endpoint displacements transformed by the estimated nonparametric transfer functions and $E[]$ is the expected value operator. As reported previously (Perreault et al. 2001), these nonparametric models fit the data well. The R^2 for all collected trials was 94.6±2.6% when the nonparametric models were fitted to the 30 s of available data. The cross-validation accuracy of the nonparametric models was obtained by using a model estimated

from the first 15 s of data to predict the force response to the perturbation applied during the last 15 s. Under these circumstances, the R^2 for the cross-validation data was lower than that for the fitted data by only 1.0±2.4%, indicating that the nonparametric estimates were robust. As a result, the full 30 s of data was used in the subsequent analyses.

$$R^2 \equiv 1 - \frac{\sum_{i\in[x,y]} E\left[\left(f_i(t) - \hat{f}_i(t)\right)^2\right]}{\sum_{i\in[x,y]} E\left[f_i(t)^2\right]} \tag{2}$$

Coherence estimates were used to determine frequency ranges where the linear approximation of the endpoint dynamics fit the data well. Coherence ranges from 0 to 1, with regions of low coherence indicating insufficient input power, significant system nonlinearities, noise, or contributions from unmeasured inputs (Marmarelis and Marmarelis 1978). The *multiple* coherence functions for the dynamic stiffness estimates show the degree to which output forces along each axis of measurement can be linearly predicted using both input displacements. They also indicate the frequencies over which a linear model accurately characterizes the endpoint stiffness dynamics. *Partial* coherence provides an estimate of the linearity of the relationship between single inputs and outputs. These estimates are equivalent to ordinary coherence estimates after the effects of all other inputs have been removed from both the input and output of interest (Bendat and Piersol 1986).

Parameterization of transfer functions

Previous experimental studies have shown that, for small perturbations, each of the SISO systems contributing to the net endpoint stiffness dynamics of the human arm can be approximated by a system having inertial (I), viscous (B) and elastic (K) parameters (Dolan et al. 1993; Tsuji et al. 1995), as shown in Eq. 3. This parametric approximation to the endpoint dynamics was also adequate for the experimental data obtained here. Inertial, viscous and elastic parameters were fit to each of the nonparametric transfer functions using a Nelder-Mead multi-dimensional optimization algorithm in Matlab (The Mathworks, Natick, MA). During the fitting process, the squared error between the nonparametric and parametric transfer functions was weighted across frequencies by the partial coherence to reduce the influence of poorly estimated portions of the transfer functions.

We assumed that endpoint inertia was invariant across all trials at each arm posture. The most reliable inertial estimates are obtained at rest, where the relative contributions of endpoint viscosity and elasticity are small. Therefore, endpoint inertia, viscosity and elasticity were estimated for the passive trials, but inertia was held constant at this passive estimate when estimating the endpoint viscosity and elasticity during the active trials. The resulting parameterized system had the form given by Eq. 4. I_{end}, B_{end}, and K_{end} correspond to the endpoint inertia, viscosity, and elasticity matrices, respectively. These components of dynamic stiffness are directionally dependent, meaning that the resistance they provide to external perturbations of hand posture depends upon the orientation of the perturbation. This dependence on direction can be represented graphically by transforming the inertial, viscous and elastic matrices into ellipses, as was first demonstrated by Mussa-Ivaldi et al. (1985). The major axis of the each ellipse denotes the direction along which that component of the endpoint response provides the most resistance to displacements of posture.

$$H_{ij}(s) = I_{ij}s^2 + B_{ij}s + K_{ij}, \text{ where } s = 2\pi f\sqrt{-1} \tag{3}$$

$$\begin{aligned}
&[I_{end}]\begin{bmatrix}\ddot{x}\\ \ddot{y}\end{bmatrix} + [B_{end}]\begin{bmatrix}\dot{x}\\ \dot{y}\end{bmatrix} + [K_{end}]\begin{bmatrix}x\\ y\end{bmatrix} = \begin{bmatrix}f_x\\ f_y\end{bmatrix}; \text{ where}\\
&[I_{end}] = \begin{bmatrix}I_{xx} & I_{xy}\\ I_{yx} & I_{yy}\end{bmatrix},\\
&[B_{end}] = \begin{bmatrix}B_{xx} & B_{xy}\\ B_{yx} & B_{yy}\end{bmatrix},\\
&[K_{end}] = \begin{bmatrix}K_{xx} & K_{xy}\\ K_{yx} & K_{yy}\end{bmatrix}
\end{aligned} \tag{4}$$

The dynamic stiffness of the elbow and shoulder joints and the coupling stiffnesses acting between these joints provide insight to the physiological mechanisms underlying the measured endpoint behavior. These joint-level dynamic stiffness parameters were computed directly from the estimated endpoint parameters using the following transforms:

$$\begin{aligned}
K_{jnt} &= J^T \cdot K_{end} \cdot J + \frac{\partial J^T}{\partial \Theta} F_{end}\\
B_{jnt} &= J^T \cdot B_{end} \cdot J\\
I_{jnt} &= J^T \cdot I_{end} \cdot J\\
J &= \begin{bmatrix} -l_h \sin(\theta_s) - l_f \sin(\theta_s + \theta_e) & -l_f \sin(\theta_s + \theta_e)\\ l_h \cos(\theta_s) + l_f \cos(\theta_s + \theta_e) & l_f \cos(\theta_s + \theta_e)\end{bmatrix}
\end{aligned} \tag{5}$$

where J is the Jacobian relating differential changes in joint rotation to differential changes in endpoint displacement, l_h and l_f are the lengths of the humerus and forearm, θ_s and θ_e are the shoulder and elbow angles, and F_{end} is the steady state endpoint force vector. The additional term in the elastic stiffness transformation is due to the geometry of the arm and the constant forces exerted voluntarily by the subject and acting at the endpoint (McIntyre et al. 1996). The Jacobian can also be used to obtain shoulder and elbow joint torques (TQ) from the measured endpoint forces as shown in Eq. 6:

$$\begin{bmatrix}TQ_s\\ TQ_e\end{bmatrix} = J^T\begin{bmatrix}f_x\\ f_y\end{bmatrix} \tag{6}$$

Parameter error estimation

The estimation errors associated with the nonparametric system identification algorithm and the subsequent parameter fits were evaluated using Monte Carlo simulations to replicate the results of each trial. These techniques are useful when repeated measurements are not practical (Hamming 1986; Press et al. 1992; Politis 1998; Ljung 1999). For each trial, the estimated nonparametric transfer functions were assumed to represent the "true" endpoint stiffness dynamics. One hundred simulated data sets were generated by convolving these same four transfer functions with different endpoint displacements (each independent but with the same statistical properties as the experimental displacements), creating simulated endpoint forces. Randomly generated "measurement" noise, matched to the power spectra and standard deviation of the experimental measurement noise, was also added to each of the simulated force responses. The system identification and parameter fitting algorithms described above were applied to each of the simulated data sets. Confidence intervals on the parameter estimates for each trial were then estimated using the standard deviation of these parameters across all 100 simulated trials. Recent results have demonstrated that this approach accurately replicates the variability observed during repeated experimental measurements of endpoint stiffness (Pierre and Kirsch 2003). For our data, the average parameter standard deviations for the inertial, viscous and elastic estimates were 0.033 N·s^2/m, 1.12 N·s/m, and 24.0 N/m, respectively, across all subjects and all endpoint forces. The maximum magnitudes for these parameters were approximately

3 N·s^2/m, 40 N·s/m, and 1,500 N/m, respectively, across all subjects and forces.

Total dynamic response: fundamental modes

The parameter ellipses introduced above describe components of the endpoint response to external disturbances. The overall response to these disturbances depends upon the relative values of all of these parameters, as well as on the temporal properties of the disturbance. Therefore, a modal analysis was performed to investigate the net dynamic behavior of the arm in response to arbitrary endpoint disturbances.

The fundamental modes of a system are an orthogonal set of transient responses that span the space of all possible responses. Any transient response of a linear system is simply a linear combination of its fundamental modes (D'Azzo and Houpis 1995), hence, the fundamental modes of a system fully describe its dynamic behavior. These modes can be computed directly from the eigenvalues and eigenvectors of the system state matrix. Equation 7 gives the state-space equations representing the linearized endpoint stiffness dynamics, where A is the state matrix and I is the identity matrix. This fourth-order model of dynamic endpoint stiffness has four corresponding modes. When all eigenvalues of the state matrix **A** are unique, the i^{th} mode is given by Eq. 8, where ε_i is the i^{th} eigenvector of the state matrix and λ_i is the corresponding eigenvalue.

$$\dot{x} = Ax + Bu$$
$$y = Cx + Du$$
where
$$A = \begin{bmatrix} 0 & I \\ -I_{end}^{-1} \cdot K_{end} & -I_{end}^{-1} \cdot B_{end} \end{bmatrix}, \quad (7)$$
$$B = \begin{bmatrix} 0 \\ I_{end}^{-1} \end{bmatrix}, C = [I \quad 0], \text{and } D = 0$$

$$m_i(t) = \varepsilon_i e^{\lambda_i t} \quad (8)$$

Total dynamic response: endpoint stability

The endpoint dynamics are stable when all of the state matrix eigenvalues have negative real parts. Equation 8 demonstrates that under these conditions, the fundamental modes of the system decay exponentially. When the eigenvalues are real the decay is exponential. When the eigenvalues are complex, i.e., have non-zero imaginary components, this decay is in the form of damped oscillations. The rate of decay relative to the frequency of the oscillations is described by the damping ratio, ζ, of the mode, which is defined in Eq. 9 for a specific eigenvalue, λ_i. Damping ratios range from 0.0 to 1.0. A mode with a damping ratio of 0.0 is said to be undamped, and has oscillations that do not decay over time. A damping ratio of 1.0 indicates that the mode does not oscillate.

$$\zeta_i = \sqrt{\frac{1}{\left(\frac{\mathrm{Im}(\lambda_i)}{\mathrm{Re}(\lambda_i)}\right)^2 + 1}} \quad (9)$$

Results

Graphical representation of dynamic endpoint stiffness

The viscoelastic properties of the arm depended on endpoint location and the level of voluntary activation. Figure 3 illustrates the endpoint inertial, viscous and elastic parameters for a typical subject. These ellipses are positioned at a location proportional to the force magnitude and in the direction that the subject was exerting this force against the manipulator. The thin straight lines indicate arm orientation, with the hand located at the center of each group of ellipses. Inertia was

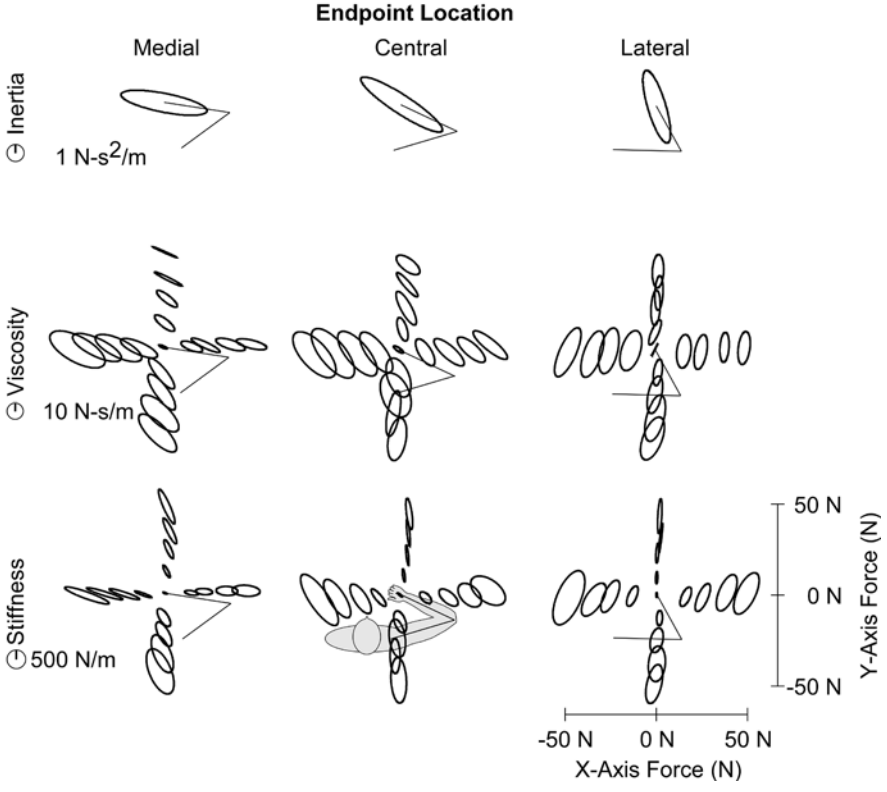

Fig. 3 Graphical representation of estimated inertial, viscous and elastic parameters for all trials of a single subject (#4). Inertia was assumed constant for all experimental trials at a given arm posture. Hence, only one inertia ellipse is shown for each of the three endpoint locations studied. Separate stiffness and viscosity ellipses are shown for each trial. The position of the ellipse center is proportional to the mean force exerted during the trial. The *thin straight lines* indicate arm orientation

assumed constant for all voluntary forces generated at a given endpoint location; hence, only one inertia ellipse is shown for each of the endpoint locations studied. These estimates were in close agreement to those predicted from anthropomorphic measurements (Winter 1990); magnitudes differed by an average of 2.3±9.5% and orientations by 0.4±3.3% across all arm postures and all subjects. This degree of agreement is well within the accuracy that can be expected when estimating limb segment inertias via simple scaling techniques (Hinrichs 1985). Endpoint inertia was greatest along an axis similar to that of the forearm, as has been reported previously (Mussa-Ivaldi et al. 1985; Flash and Mussa-Ivaldi 1990; Dolan et al. 1993; Tsuji et al. 1995). In general, the orientation of the endpoint inertia was different than that of the endpoint viscosity and elasticity ellipses. The orientation the elastic and viscous ellipses also differed for certain endpoint force loads, such as $+Y$ loads at the central and medial endpoint positions. This is in contrast to previous findings under no-load and very low-load conditions (Dolan et al. 1993; Tsuji et al. 1995; Stroeve 1999). These differences in orientation for the different parameter ellipses indicate that the maximum arm resistance to external disturbances will be dependent on the temporal structure of the disturbance in addition to the well documented directional structure (Mussa-Ivaldi et al. 1985; Dolan et al. 1993; Tsuji et al. 1995; Gomi and Osu 1998; Perreault et al. 2001).

Changes in endpoint viscosity with force

The relationship between endpoint force and endpoint viscosity was nonlinear. This is in contrast to the linear relationship between endpoint force and endpoint elasticity (Perreault et al. 2001), but consistent with single joint measurements which showed that joint viscosity is proportional to the square root of the joint torque (Weiss et al. 1988; Kearney and Hunter 1990; Kirsch and Rymer 1992). Based on these earlier findings, the nonlinear endpoint viscosity-force relationship was approximated by Eq. 10, which assumes that viscosity scales with the square root of endpoint force. Figure 4 shows a typical endpoint viscosity-force relationship for a single subject at the central arm posture. Figure 4A shows the relationship between the endpoint viscosity parameters and endpoint forces exerted along the X-axis; Fig. 4B shows how these same parameters vary with Y-axis forces. The solid circles show the experimental data, and the solid lines show the model predictions (Eq. 10) for forces that are aligned exactly with the X- and Y-axes. Standard deviation error bars for the data points are also plotted, but in many cases these are smaller than the circles used to represent the data. The average r^2 for this model was 0.79±0.12. The r^2 values for a single subject are provided in Fig. 4. Note that the r^2 values reported for each component of the endpoint viscosity matrix are identical for forces along the X- and Y-axes because Eq. 10 was fit to all data simultaneously. The discrepancies between the experimental data points and the model predictions are due to both model errors and the fact that some of the experimental forces were not exactly aligned with the X- and Y-axes, but rather had small off-axis components.

$$B_{ij}^{end} = \alpha_0 + \alpha^{+}_{\sqrt{Fx}}\sqrt{\left|F_x^{+}\right|} + \alpha^{+}_{\sqrt{Fy}}\sqrt{\left|F_y^{+}\right|} + \alpha^{-}_{\sqrt{Fx}}\sqrt{\left|F_x^{-}\right|} + \alpha^{-}_{\sqrt{Fy}}\sqrt{\left|F_y^{-}\right|} \quad (10)$$

Changes in joint viscosity with torque

The joint viscosity–joint torque relationship could not be shown to be independent of arm posture. Recent results have demonstrated that joint elasticity–joint torque curves are nearly posture independent during force regulation tasks, such as those used in this study (Perreault et al.

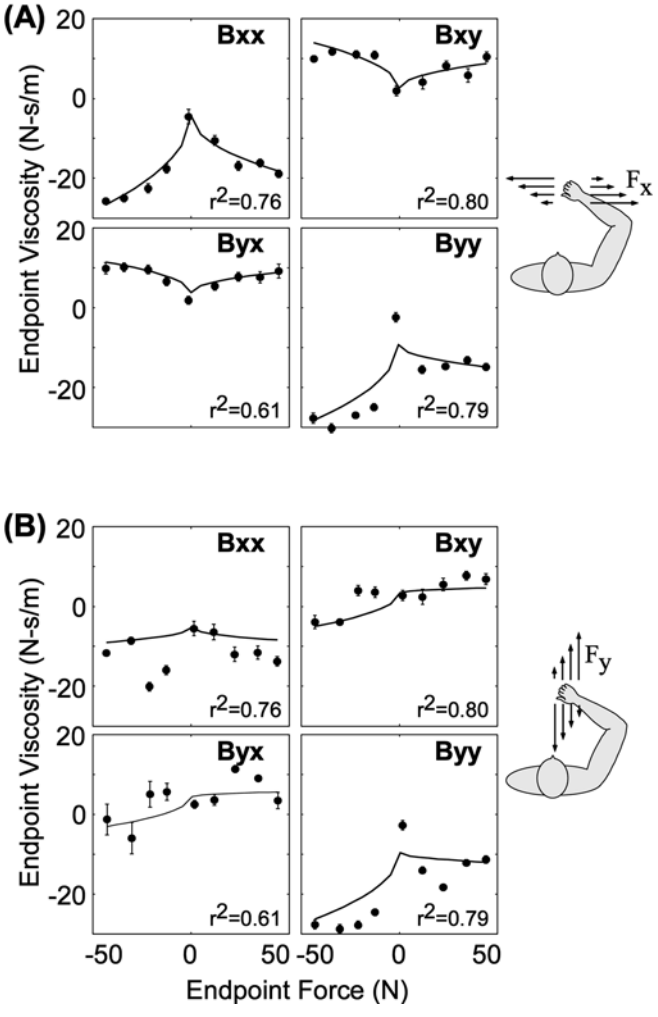

Fig. 4A, B Variations in endpoint viscosity with endpoint force for a single subject (#4, central posture). **A** shows how each component of the endpoint viscosity matrix scaled with changes in endpoint force along the X-axis. **B** shows how these parameters varied with changes in force along the Y-axis. *Error bars* indicate ±1 SD. The r^2 values in each panel were obtained by fitting the estimated parameters to Eq. 10. Because all data were fit simultaneously, the r^2 values in **A** and **B** are identical

2001). The postural invariance of joint viscosity regulation was examined by attempting to model the joint viscosity–joint torque relationship measured at all endpoint positions with a single set of parameters. Extending the results of single joint studies and the relationship between endpoint force and endpoint viscosity described above, we assumed that joint viscosities scaled with the square root of joint torque. Equation 12 shows the model that was fit to the data. The average r^2 for this model was 0.56; elbow joint viscosity was predicted most accurately (r^2=0.77), followed by shoulder joint viscosity (r^2=0.56), and the cross-joint viscosities (r^2=0.46). In general, the accuracy of these fits was poor relative to similar fits for joint elasticity (Perreault et al. 2001). However, based upon the limited data set, it is not possible to determine if our inability to describe the joint viscosity-joint torque data with a posture independent model is due to the existence of a posture-dependent relationship or an inappropriate choice of model structure. Additional data would be required to resolve this issue.

$$B_{ij}^{\text{Joint}} = \alpha_0 + \alpha^{+}_{\sqrt{TQ_s}}\sqrt{|TQ_s^{+}|} + \alpha^{+}_{\sqrt{TQ_e}}\sqrt{|TQ_e^{+}|} + \alpha^{-}_{\sqrt{TQ_s}}\sqrt{|TQ_s^{-}|} + \alpha^{-}_{\sqrt{TQ_e}}\sqrt{|TQ_e^{-}|} \tag{11}$$

Endpoint dynamics

Response to perturbations

The response to arbitrary perturbations was examined by simulating the endpoint trajectory that would be generated in response to a series of unit force impulses (1 N) applied at the hand, assuming that the experimentally determined elastic, viscous, and inertial matrices capture the arm dynamics. Figure 5A illustrates a sample endpoint trajectory for one such simulation. This particular perturbation was approximately perpendicular to the forearm and the endpoint position oscillated approximately along the direction of the applied perturbation. Figure 5B and C show a series of such trajectories representing the endpoint dynamics estimated during two particular experimental conditions. The arrows in the center of each series represent the directions along which the fundamental modes oscillate. Figure 5B shows the endpoint trajectories for an endpoint force condition where the inertial, viscous and elastic ellipses were oriented approximately in the same direction. Under these conditions, external perturbations cause the arm to oscillate primarily along the minor axes of these ellipses rather than along the direction of the perturbation. This corresponds to the small axes of the parameter ellipses, the smallest mode of the system, and the direction for which the endpoint is least resistant to perturbations. Figure 5C shows the trajectories for a condition when the inertial, viscous, and elastic ellipses are not co-oriented. Under these conditions, the net response to external perturbations could not be predicted easily from the parameter ellipses. Rather, the endpoint response had significant components along both of the modal axes for perturbations in most directions. These results demonstrate the need to examine the net dynamic response of the arm in order to describe the response to externally applied perturbations.

Endpoint stability

The endpoint dynamics remained stable for all force regulation tasks examined in all subjects. Stability was quantified by computing the eigenvalues of the state matrix, A, described in Eq. 7. We found that the state matrix for every trial had eigenvalues with negative real parts. Further, the damping ratios of the minimally damped modes remained fairly constant (0.26±0.08). Because the eigenvalues appeared in complex conjugate pairs, the four system modes had only two distinct damping ratios. Figure 6 summarizes the damping ratios estimated for all subjects. Figure 6A shows the histograms for the damping ratios from all experimental trials. The damping ratios for the minimally damped modes are shown on the top and those for the maximally damped modes on the bottom. The bold dashed lines indicate the median damping ratios ($\zeta_{\min}$=0.25, $\zeta_{\max}$=0.47), and the thin dashed lines encompass 90% of the observed results. It is evident that there is much less dispersion in the damping ratios for the minimally damped modes than for the maximally damped modes. Figure 6B shows the variations in the damping ratio of the minimally damped mode as a function of both endpoint location and subject. The median differences were small at different endpoint positions and for different subjects. The maximal difference in the inter-subject medians was $\Delta\zeta$=0.06. Some changes in damping ratio were observed as a function of endpoint force direction, but these changes were small relative to the observed regularity (0.13 maximum difference, not shown). Figure 6C demonstrates the degree of oscillations that can be expected from damping ratios in the observed range. All responses are normalized with respect to both amplitude and oscillation frequency. The median response is shown in bold. The lighter traces correspond to damping ratios that bound 90% of the observed results (ζ=0.14 and ζ=0.39). Note that the physical effect of even this range is small.

Discussion

This work investigated how the multijoint stability of the human arm is regulated across changes in arm posture and voluntary force generation. Stability was quantified using estimates of dynamic endpoint stiffness, which describes the dynamic relationship between externally applied displacements of the hand and the forces generated in response. Hence, it characterizes the mechanical interface that humans use to interact with their environment and is thought to provide a quantitative measure of postural stability (Hogan 1985; Dolan et al. 1993; Lacquaniti et al.

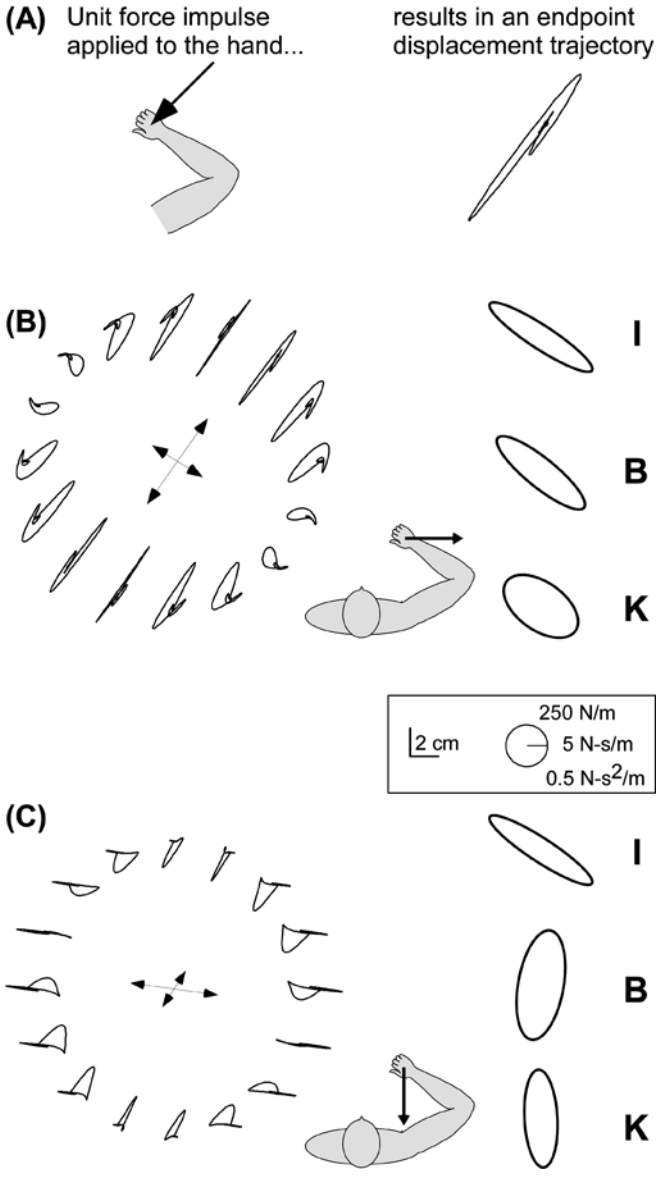

Fig. 5A–C Simulated transient responses for graphically representing endpoint dynamics. **A** illustrates the simulated endpoint trajectory in response to an applied force impulse. The *left portion* shows the orientation of the force impulse and the right portion shows the corresponding endpoint trajectory. **B** and **C** show a series of such trajectories simulated using the dynamic stiffness parameters estimated from a single subject (#4; central posture) during two different experimental trials in which voluntary forces were generated at 30% MVC along the $+X$ **(B)** and $-Y$ axes **(C)**. The direction of voluntary force generation is indicated by the orientation of the *arrow* attached to the subject's arm. Sixteen force orientations were simulated for each condition; each *trajectory* shows the displacements resulting from force impulses directed from the center of the trajectory towards the center of the ring. The *ellipses* to the right of each ring show the estimated endpoint inertia, viscosity, and elasticity used in the simulation. The *arrows* in the center of the rings indicate the orientations of the minimally and maximally damped system modes, with the *larger arrow* representing the minimally damped mode. Note that most of the computed eigenvalues occurred in complex conjugate pairs. Each member of the pair has the same mode orientation and damping ratio; hence, only two mode orientations need to be illustrated

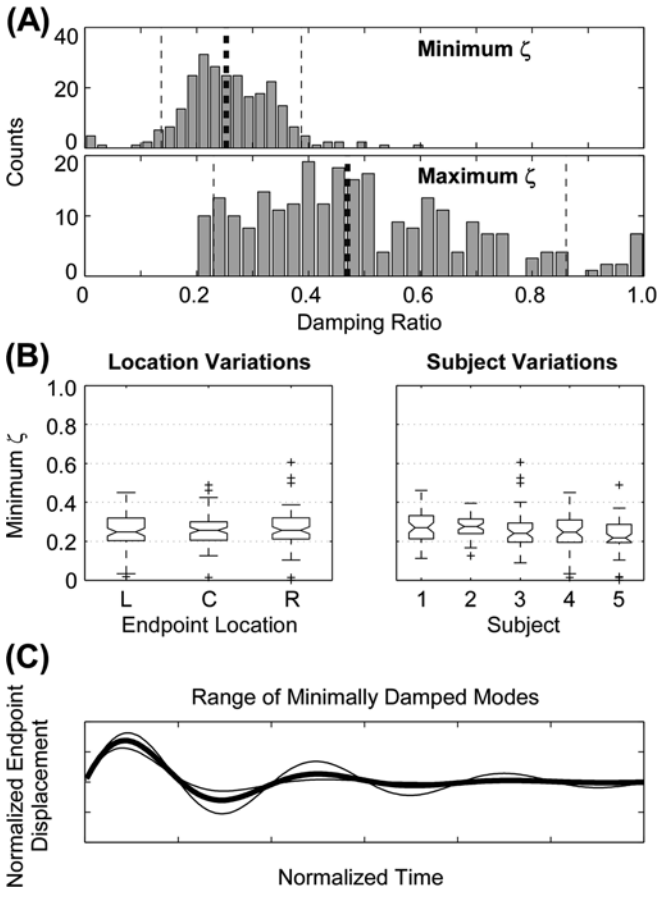

Fig. 6A–C Summary of the damping ratio for the modes characterizing the endpoint stiffness dynamics. **A** shows the histograms for the damping ratios estimated from all subjects in all experimental trials (N=255). The damping ratios for the minimally damped modes are shown *on the top* and those for the maximally damped modes *on the bottom*. The *bold dashed lines* indicate the median damping ratios and the *thin dashed lines* encompass 90% of the observed results. **B** shows the variations in the damping ratio of the minimally damped mode as a function of both endpoint location and subject. **C** demonstrates the degree of oscillations that can be expected from damping ratios in the observed range. All responses are normalized with respect to both amplitude and oscillation frequency. The median response is shown in *bold*. The *lighter traces* correspond to damping ratios that bound 90% of the observed results

1993; Tsuji et al. 1995; Gomi and Osu 1998). A previous study in our lab investigated how the elastic component of dynamic endpoint stiffness changes during force regulation tasks (Perreault et al. 2001). The current work extends those results by characterizing the viscous and inertial contributions to endpoint stiffness and by investigating how these components combine to generate the net limb stability and response to externally applied perturbations.

Regulation of limb viscosity

Endpoint viscosity increased nonlinearly with increasing endpoint forces. Viscosity increases were approximately proportional to the square root of the endpoint force increase. This is in contrast to the linear relationship

between endpoint elasticity and endpoint force (Gomi and Osu 1998; Perreault et al. 2001). The nonlinear viscosity-force characteristic is consistent with numerous single joint studies that demonstrated a similar nonlinear relationship between joint torque and joint viscosity (Weiss et al. 1988; Kirsch and Rymer 1992; Zhang and Rymer 1997). In their multi-joint study, Gomi and Osu (1998) also observed a nonlinear dependence of joint viscosity on joint torque but did not collect data over a large enough range of joint torques to determine the nature of this relationship.

The results of numerous studies suggest that the nonlinear relationship between force and viscosity arises from intrinsic muscle properties rather than through reflex mediated changes in muscle activation. Similar nonlinearities have been observed during the rise of tension in individual muscle fibers (Cecchi et al. 1997; Bagni et al. 1998), and during steady contractions of deafferented whole muscle preparations activated using both electrical stimulation and natural activation via the crossed-extension reflex (Kirsch et al. 1994). Furthermore, techniques for separately identifying the intrinsic and reflex contributions to single joint impedance have been used to demonstrate that the nonlinear joint viscosity-torque relationship found in humans persists even once the contributions of stretch sensitive reflexes have been considered (Kearney et al. 1997; Zhang and Rymer 1997). Although neither direct measurements nor indirect estimates of the intrinsic muscle properties were made in this study, it is known that continuous movements can reduce stretch reflex gain and H-reflex responses (Capaday and Stein 1986; Stein and Kearney 1995). Hence, it is likely that the random perturbations used to estimate limb impedance emphasized the contributions of intrinsic muscle properties to limb impedance and that the nonlinear force-viscosity relationship was a direct result of these properties.

The mechanisms underlying the nonlinear viscosity-force relationship are unclear. One possibility is that the viscous response to stretch increases nonlinearly with increases in mean firing rate. Increases in voluntary force generation are mediated via increases in motor unit recruitment and rate modulation. The resultant forces from individual motor units and groups of motor units scale nearly linearly during both isometric (Perreault et al. 2003) and transient (Nichols and Houk 1976) conditions. However, the forces generated in response to transient perturbations do not scale linearly with muscle force when that force is regulated solely by changes in rate modulation (Nichols and Houk 1976). This is reflected in the fact that the force velocity properties of isolated muscle also scale nonlinearly when force is modulated via changes in stimulation rate (Joyce et al. 1969) and may also explain activation-dependent changes in maximum shortening velocity observed during voluntary contractions (Chow and Darling 1999). An alternative explanation is that the observed nonlinear force-velocity relationship reflects an inability of the parallel visco-elastic structure used in this study to capture specifics of the underlying muscle mechanics (Perreault et al. 2000), causing unmodeled structures, such as in-series tendon compliance, to influence how changes in muscle viscosity are transmitted to the endpoint. Tendon compliance can result in curvature of the elasticity-force relationship at higher force levels (Huyghues-Despointes et al. 2003) and may have a similar effect on the estimation of viscosity-force relationships at the force levels considered in the work.

The orientation of the maximal endpoint viscosity depended upon the direction in which voluntary forces were generated, as reported previously for endpoint elasticity (Gomi and Osu 1998; Perreault et al. 2001). However, in contrast to previous findings (Dolan et al. 1993; Tsuji et al. 1995), the elasticity and viscosity orientations estimated in this study were not always co-aligned. Previous studies that reported the orientations of endpoint elasticity and viscosity focused on passive conditions or forces less than 2% of the maximum forces considered in this work. Hence, our results reflect the behaviour of endpoint elasticity and viscosity over a wider range of voluntary forces.

These differences in elasticity and viscosity orientation may result from the nonlinear dependence of endpoint viscosity on endpoint force or may suggest independent mechanisms for regulating the orientation of limb elasticity and viscosity. The latter suggestion is in agreement with the results of Lacquaniti et al. (1993) who provided evidence for independent elasticity and viscosity control during the preparatory stages of ball catching. Their results showed that prior to impact, endpoint viscosity orientation is rotated to become more in line with the direction of the expected perturbation even though endpoint elasticity orientation remains invariant. These results, coupled with the finding that it is difficult to voluntarily modify elastic stiffness orientation during force regulation tasks (Perreault et al. 2002), suggest that during the maintenance of posture, the neural control over endpoint viscosity orientation may be more flexible than that over endpoint elasticity orientation.

Response to transient perturbations

The inertial, viscous and elastic properties of the arm were combined using a state-space formulation to investigate the net endpoint dynamics. This allowed the endpoint trajectories generated in response to small perturbations of the arm to be simulated. Simulation results demonstrated that when the parameter ellipses are co-oriented force impulses applied to the hand result in endpoint oscillations predominantly along the minor axis of the parameter ellipses (Fig. 5B). The orientation of these oscillations was nearly independent of the endpoint disturbance orientation. When the parameter ellipses were not co-oriented, the endpoint response became more complex (Fig. 5C); oscillations displayed more variation with respect to the endpoint disturbance orientation, and tended not to oscillate along a single axis. Hence, these trajectories

could not be predicted solely from the orientations of the parameter ellipses.

These results imply that the response to postural perturbations can be understood only if the net dynamics are considered. This is particularly true when the endpoint parameter ellipses are not co-oriented. Early studies of endpoint stiffness were restricted to the static components of stiffness (Mussa-Ivaldi et al. 1985; Flash and Mussa-Ivaldi 1990; McIntyre et al. 1996), and the later studies that characterized the full dynamic response did little to integrate the effects of inertia, viscosity, and elasticity (Dolan et al. 1993; Lacquaniti et al. 1993; Tsuji et al. 1995; Gomi and Osu 1998). One recent exception is the modeling study of Stroeve (1999), although this did not examine the large range of voluntarily generated forces tested in this work. It is well documented that during posture, endpoint inertia and elasticity commonly have different orientations (Mussa-Ivaldi et al. 1985; Flash and Mussa-Ivaldi 1990; Dolan et al. 1993; Tsuji et al. 1995). Our results show that that endpoint viscosity and elasticity may also have different orientations, indicating that in many postural situations, a full dynamic analysis will be needed to understand the response to external perturbations and the stability that results from this response.

Endpoint stability

By considering the dynamic response of the arm, we were able to demonstrate that arm posture remained stable under all tested experimental conditions. Similar findings have been reported by McIntyre et al. (1996) and recently by Franklin et al. (2003), although both of those studies were restricted to the elastic components of endpoint stiffness. McIntyre (1996) demonstrated how endpoint forces directed toward the shoulder and elbow joints decrease arm stability but that this load-dependent decrease in stability could be countered by the increase in endpoint elasticity that occurs with increasing voluntary force generation. Our results extend those findings to show that dynamic stability, which characterizes the total response to external perturbations, is also maintained in the presence of large endpoint force loads.

The degree of dynamic stability was nearly invariant across all subjects, arm postures and voluntarily generated forces tasks, supporting our hypothesis that whole limb stability would be tightly regulated over a wide range of operating conditions. Dynamic stability was quantified by examining the damping ratios of the modes characterizing the estimated endpoint mechanics. We found that the minimally damped modes had a damping ratio that was nearly invariant across all experimental trials; there were minimal changes in the damping ratio with changes in force magnitude, force direction, or endpoint location. These results suggest that, during force regulation tasks, the maximum number of oscillations due to an external disturbance is nearly independent of arm posture and external force. Similar results have been observed in the study of single joint mechanics (Agarwal and Gottlieb 1977; Weiss et al. 1988; Sinkjaer and Hayashi 1989). Our results are the first to extend these findings to the case of multi-joint dynamics.

The consistent regulation of limb stability during force regulation tasks may arise from the intrinsic properties of the arm muscles used to generate the target endpoint forces. At the single joint level, damping will remain constant if joint viscosity increases in proportion to the square root of joint elasticity (Kearney and Hunter 1990). A similar relation between endpoint viscosity and endpoint elasticity was observed in this study and appears to arise via the intrinsic properties of the muscles generating the specified endpoint forces (see "Regulation of limb viscosity", above). This fundamental relationship between elasticity and viscosity during isometric force regulation tasks may provide an intrinsic mechanism for maintaining limb stability once an appropriate set of muscles is chosen to generate the necessary endpoint forces.

It is likely that the minimal damping ratios and the corresponding limb stability observed in this study represent a lower limit on the multijoint damping that can be expected during more complex tasks. Force regulation tasks require subjects to exert steady forces against a stable, non-compliant manipulator. Hence, stability is provided predominantly by the manipulator rather than by the human limb. Limb damping is likely to increase during tasks in which the arm mechanics are the dominant factor influencing net stability. Indeed, the damping constant of individual joints is known to increase during tasks that result in significant co-contraction (Milner and Cloutier 1998), increased reflex gain (Sinkjaer and Hayashi 1989), or movement (Bennett et al. 1992).

Conclusions

This study examined the modulation of limb stiffness dynamics during force regulation tasks. Our results demonstrated the importance of considering the dynamic response of the limb rather than just the response to steady state perturbations. By assessing the dynamic response of the limb, we were able to show that limb stability remains nearly invariant across a range of arm postures and voluntarily generated forces. This regulation appears to arise via the intrinsic properties of the muscles contributing to the force regulation task and may represent a lower bound on the stability of limb mechanics that can be expected during movement or tasks involving interactions with an unstable environment.

References

Acosta AM, Kirsch RF, Perreault EJ (2000) A robotic manipulator for the characterization of two-dimensional dynamic stiffness using stochastic displacement perturbations. J Neurosci Methods 102:177–186

Agarwal GC, Gottlieb GL (1977) Compliance of the human ankle joint. J Biomech Eng 99:166–170

Bagni MA, Cecchi G, Cecchini E, Colombini B, Colomo F (1998) Force responses to fast ramp stretches in stimulated frog skeletal muscle fibres. J Muscle Res Cell Motil 19:33–42
Bendat JS, Piersol AG (1986) Random data: analysis and measurement procedures. Wiley, New York
Bennett DJ, Hollerbach JM, Xu Y, Hunter IW (1992) Time-varying stiffness of the human elbow joint during cyclic voluntary movement. Exp Brain Res 88:433–442
Capaday C, Stein RB (1986) Amplitude modulation of the soleus H-reflex in the human during walking and standing. J Neurosci 6:1308–1313
Cecchi G, Bagni MA, Cecchini E, Colombini B, Colomo F (1997) Crossbridge viscosity in activated frog muscle fibres. Biophys Chem 68:1–8
Chow JW, Darling WG (1999) The maximum shortening velocity of muscle should be scaled with activation. J Appl Physiol 86:1025–1031
D'Azzo JJ, Houpis CH (1995) Linear control system analysis and design. McGraw-Hill, New York
Dolan JM, Friedman MB, Nagurka ML (1993) Dynamic and loaded impedance components in the maintenance of human arm posture. IEEE Trans Syst Man Cybern 23:698–709
Flash T, Gurevich I (1997) Models of motor adaptation and impedance control in human arm movements. In: Morasso P, Sanguineti V (eds) Self-organization, computational maps, and motor control. Elsevier Science, Amsterdam, pp 423–481
Flash T, Mussa-Ivaldi FA (1990) Human arm stiffness characteristics during the maintenance of posture. Exp Brain Res 82:315–326
Franklin DW, Milner TE (2003) Adaptive control of stiffness to stabilize hand position with large loads. Exp Brain Res 152:211–220
Gomi H, Osu R (1998) Task-dependent viscoelasticity of human multijoint arm and its spatial characteristics for interaction with environments. J Neurosci 18:8965–8978
Hamming RW (1986) Numerical methods for scientists and engineers. Dover, New York
Hinrichs RN (1985) Regression equations to predict segmental moments of inertia from anthropometric measurements: an extension of the data of Chandler et al. (1975). J Biomech 18:621–624
Hogan N (1985) The mechanics of multi-joint posture and movement control. Biol Cybern 52:315–331
Huyghues-Despointes CM, Cope TC, Nichols TR (2003) Intrinsic properties and reflex compensation in reinnervated triceps surae muscles of the cat: effect of activation level. J Neurophysiol 90:1537–1546
Joyce GC, Rack PM, Westbury DR (1969) The mechanical properties of cat soleus muscle during controlled lengthening and shortening movements. J Physiol 204:461–474
Kearney RE, Hunter IW (1990) System identification of human joint dynamics. CRC Crit Rev Biomed Eng 18:55–87
Kearney RE, Stein RB, Parameswaran L (1997) Identification of intrinsic and reflex contributions to human ankle stiffness dynamics. IEEE Trans Biomed Eng 44:493–504
Kirsch RF, Rymer WZ (1992) Neural compensation for fatigue-induced changes in muscle stiffness during perturbations of elbow angle in human. J Neurophysiol 68:449–470
Kirsch RF, Boskov D, Rymer WZ (1994) Muscle stiffness during transient and continuous movements of cat muscle: perturbation characteristics and physiological relevance. IEEE Trans Biomed Eng 41:758–770
Lacquaniti F, Carrozzo M, Borghese NA (1993) Time-varying mechanical behavior of multijointed arm in man. J Neurophysiol 69:1443–1463
Ljung L (1999) System identification theory for the user. Prentice-Hall, Upper Saddle River, NJ
Mann KA, Werner FW, Palmer AK (1989) Frequency spectrum analysis of wrist motion for activities of daily living. J Orthop Res 7:304–306
Marmarelis PZ, Marmarelis VZ (1978) Analysis of physiological systems. Plenum Press, New York
McIntyre J, Mussa-Ivaldi FA, Bizzi E (1996) The control of stable arm postures in the multi-joint arm. Exp Brain Res 110:248–264
Milner TE, Cloutier C (1998) Damping of the wrist joint during voluntary movement. Exp Brain Res 122:309–317
Mussa-Ivaldi FA, Hogan N, Bizzi E (1985) Neural, mechanical, and geometric factors subserving arm posture in humans. J Neurosci 5:2732–2743
Nichols TR, Houk JC (1976) Improvement in linearity and regulation of stiffness that results from actions of stretch reflex. J Neurophysiol 39:119–142
Perreault EJ, Kirsch RF, Acosta AM (1999) Multiple-input, multiple-output system identification for the characterization of limb stiffness dynamics. Biol Cybern 80:327–337
Perreault EJ, Crago PE, Kirsch RF (2000) Estimation of intrinsic and reflex contributions to muscle dynamics: a modeling study. IEEE Trans Biomed Eng 47:1413–1421
Perreault EJ, Kirsch RF, Crago PE (2001) Effects of voluntary force generation on the elastic components of endpoint stiffness. Exp Brain Res 141:312–323
Perreault EJ, Kirsch RF, Crago PE (2002) Voluntary control of static endpoint stiffness during force regulation tasks. J Neurophysiol 87:2808–2816
Perreault EJ, Day SJ, Hulliger M, Heckman CJ, Sandercock TG (2003) Summation of motor unit forces in cat soleus during experimentally simulated recruitment. J Neurophysiol 89:738
Pierre MC, Kirsch RF (2003) Measurement and reliability of 3D end-point stiffness of the human arm. In: Proc. 25th IEEE/EMBS Conf., Cancun, pp 1433–1436
Politis DN (1998) Computer-intensive methods in statistical analysis. IEEE Signal Process Mag 15:39–55
Press W, Flannery BP, Teukolsky SA, Vetterling WT (1992) Numerical recipes in C. Cambridge University Press, New York
Sinkjaer T, Hayashi R (1989) Regulation of wrist stiffness by the stretch reflex. J Biomech 22:1133–1140
Stein RB, Kearney RE (1995) Nonlinear behavior of muscle reflexes at the human ankle joint. J Neurophysiol 73:65–72
Stroeve S (1999) Impedance characteristics of a neuromusculoskeletal model of the human arm I. Posture control. Biol Cybern 81:475–494
Tsuji T, Morasso PG, Goto K, Ito K (1995) Hand impedance characteristics during maintained posture. Biol Cybern 72:475–485
Weiss PL, Hunter IW, Kearney RE (1988) Human ankle joint stiffness over the full range of muscle activation levels. J Biomech 21:539–544
Winter DA (1990) Biomechanics and motor control of movement. John Wiley, Toronto
Zhang L-Q, Rymer WZ (1997) Simultaneous and nonlinear identification of mechanical and reflex properties of human elbow joint muscles. IEEE Trans Biomed Eng 44:1192–1209